Preparation, Characterization, and Some Properties of Novel Dinuclear Complexes with a Coordinated Bridging Disulfide Bond. Crystal Structures of $\Delta_R\Lambda_S$-$[M_2(2\text{-aminoethanethiolato})_4(\text{cystamine})]^{2+}$ (M = Ir^{III}, Rh^{III})

Yoshitaro Miyashita, Narumi Sakagami, Yasunori Yamada, Takumi Konno,† and Ken-ichi Okamoto*

Department of Chemistry, University of Tsukuba, Tsukuba 305-8571

†Department of Chemistry, Faculty of Engineering, Gunma University, Kiryu, Gunma 376-8516

(Received April 27, 1998)

Novel dinuclear complexes, $[M_2(aet)_4(cysta)]^{2+}$ (M = Ir^{III} (**1**), Rh^{III} (**2**); aet = $NH_2CH_2CH_2S^-$, cysta = $NH_2CH_2CH_2SSCH_2CH_2NH_2$), were prepared by the oxidation reactions of *fac*(*S*)-[M(aet)$_3$]. The crystal structures of the complexes were determined by X-ray diffractions: **1**$Cl_2\cdot 4H_2O$, monoclinic, $P2_1/a$, a = 12.427(2), b = 8.879(1), c = 13.387(1) Å, β = 91.947(10)°, V = 1476.3(3) Å^3, Z = 2, and R = 0.031; **2**$Cl_2\cdot 2H_2O$, monoclinic, $P2_1/c$, a = 11.788(2), b = 8.485(1), c = 14.800(2) Å, β = 112.980(9)°, V = 1362.9(3) Å^3, Z = 2, and R = 0.023. In the structures of **1** and **2**, two octahedral *fac*(*S*)-[M(aet)$_3$] units are linked by a coordinated disulfide bond. Their disulfide sulfur atoms are bound to the Ir and Rh atoms more strongly than to the Co atom. Both complexes **1** and **2** take only the $\Delta_R\Lambda_S$ configuration of ten possible isomers. The electronic absorption, ^{13}C NMR, and infrared spectra exhibit characteristic behavior in relation to the disulfide bond. **1** and **2** are fairly stable in water, and their structures in solid are retained in solution. The reduction or oxidation of the dinuclear complexes causes a cleavage of the disulfide bond to afford the mononuclear thiolato or sulfinato complexes. The properties of the present complexes are also discussed in comparison with those of the mononuclear and/or polynuclear complexes with the corresponding metal ions.

In the mononuclear facial-type complexes, *fac*(*S*)-[M(aet)$_3$] (M = Co^{III}, Rh^{III}, Ir^{III}; aet = 2-aminoethanethiolate), which can function as the building blocks of the tridentate ligands and form a variety of S-bridged polynuclear complexes,[1—9] the oxidations of the thiolato group coordinated to the metal ions have given mononuclear sulfenato or sulfinato complexes, $[M(aese)_n(aesi)_{3-n}]$ (n = 0—3; aese = $NH_2CH_2CH_2SO^-$, aesi = $NH_2CH_2CH_2SO_2^-$).[10,11] Further, the equivalent oxidation on their thiolato group may form a coordinated disulfide bond, which connects two metal centers to give a dinuclear complex.[12,13] Such complexes would be of interest in the electrochemistry related to the reactivity of the disulfide bond, because of the importance of thiol-disulfide couple in biological systems. Although oxidation reactions of the mononuclear thiolatocobalt(III) complexes have been attempted, this kind of dinuclear complex has been little isolated because of the concomitant cleavage of the M–S bond.[14—16] For example, it has been shown that the oxidation reaction of $[Co(aet)(en)_2]^{2+}$ with Np(VI) in acid produces the mononuclear disulfide complex, [Co(Hcysta-*N*,*S*)$(en)_2]^{4+}$ (cysta = cystamine), via a dinuclear intermediate with the bridged cysta ligand.[14] The oxidation reaction of *fac*(*S*)-[Co(aet)$_3$] with HNO_3 results in isolation of the S-bridged tricobalt(III) complex, $[Co\{Co(aet)_3\}_2]^{3+}$, accompanied by the release of free cystamine.[16] In these reactions, the mononuclear disulfide or tricobalt(III) complexes cannot be formed without cleavage of the M–S bond. Namely, it seems that the intended complex with the disulfide bond can be obtained, if it prevents ligands from dissociating. It has been known that the M–S bonds of the Rh(III) or Ir(III) complexes are stronger than those of the Co(III) complexes. During the course of our synthetic investigation of the S-bridged polynuclear complexes with the *fac*(*S*)-[Ir(aet)$_3$] units,[2,5,7] we have found a fairly stable dinuclear Ir(III) complex with a symmetrically coordinated disulfide ligand, $[Ir_2(aet)_4(cysta)]^{2+}$ (**1**), which can be obtained by treating *fac*(*S*)-[Ir(aet)$_3$] with acid in water. A partial report on **1** has been published as a preliminary communication.[17] We report here on the complete description of the synthesis, characterization, and some properties of **1**, together with the newly prepared corresponding Rh(III) complex (**2**). Each crystal structure of complexes **1** and **2** was determined by an X-ray diffraction study. The stereochemical, spectrochemical, and electrochemical behavior of the present complexes were also discussed, together with the reactivity in this system.

Experimental

Materials. 2-Aminoetanethiol was purchased from Tokyo Kasei Kogyo Co., Inc. $RhCl_3\cdot nH_2O$ and $IrCl_3$ were purchased from N. E. Chemcat Co., Ltd. and Rare Metallic Co., Ltd., respectively. The other reagents were obtained from Wako Pure Chemical Ind. Ltd. All chemicals were of reagent grade and were used without

further purification.

Preparation of Complexes. *fac*(*S*)-[Rh(aet)$_3$],[2b,4c,11] *fac*(*S*)-[Ir(aet)$_3$],[2] *fac*(*S*)-[Rh(L-cys-*N*,*S*)$_3$],[1a,4c] and *fac*(*S*)-[Ir(L-cys-*N*,*S*)$_3$][2a] were prepared by the methods described in previous papers.

[Ir$_2$(aet)$_4$(cysta)]$^{2+}$ (1). Method A: *fac*(*S*)-[Ir(aet)$_3$] (0.30 g, 0.71 mmol) was dissolved in 10 cm^3 of 1 mol dm^{-3} HCl, and the pale brown solution was stirred at 60 °C for 15 min, whereupon it became a dark orange solution. To this solution was added 1 cm^3 of a saturated NaCl solution, followed by standing at room temperature for 1 d. The resulting dark-orange crystals (**1**Cl$_2$·4H$_2$O) were collected by filtration. A second crop of the product was collected by standing the mother liquor at room temperature for a few days. Single crystals suitable for an X-ray analysis were obtained by recrystallization from ca. 0.05 mol dm^{-3} chromium(III) chloride solution at room temperature. Similar crystals were also obtained by a reaction under a nitrogen atmosphere. Yield: 0.16 g (46%). Found: C, 14.55; H, 4.41; N, 8.40%. Calcd for [Ir$_2$(aet)$_4$(cysta)]Cl$_2$·4H$_2$O = C$_{12}$H$_{36}$N$_6$S$_6$Cl$_2$Ir$_2$·4H$_2$O: C, 14.64; H, 4.51; N, 8.54%.

Method B: To a suspension containing *fac*(*S*)-[Ir(aet)$_3$] (0.10 g, 0.24 mmol) in 2 cm^3 of water was added Ce(SO$_4$)$_2$·4H$_2$O (0.10 g, 0.25 mmol). After the mixture had been stirred at room temperature for 30 min, the resulting brown powder (**1**SO$_4$) was collected by filtration. The counter anion was exchanged by adding this powder into 5 cm^3 of a saturated NaNO$_3$ solution at 40 °C for 10 min. The resulting brown powder (**1**(NO$_3$)$_2$·3.5H$_2$O) was recrystallized from warm water by adding a few drops of a saturated NaNO$_3$ solution. Yield: 0.074 g (61%). Found: C, 14.02; H, 4.15; N, 10.79%. Calcd for [Ir$_2$(aet)$_4$(cysta)](NO$_3$)$_2$·3.5H$_2$O = C$_{12}$H$_{36}$N$_8$O$_6$S$_6$Ir$_2$·3.5H$_2$O: C, 14.02; H, 4.21; N, 10.90%.

Method C:[17] *fac*(*S*)-[Ir(aet)$_3$] (0.10 g, 0.24 mmol) was dissolved in 6 cm^3 of 0.15 mol dm^{-3} HNO$_3$, and the pale-brown solution was stirred at 60 °C for 4 h, whereupon it became a dark-orange solution. To this solution was added 1 cm^3 of a saturated NaNO$_3$ solution, followed by standing at room temperature for 1 d. The resulting dark-orange crystals (**1**(NO$_3$)$_2$·3.5H$_2$O) were collected by filtration. Yield: 0.058 g (48%).

Method D: To a suspension containing *fac*(*S*)-[Ir(aet)$_3$] (0.25 g, 0.59 mmol) in 15 cm^3 of water was added Cr(NO$_3$)$_3$·9H$_2$O (1.0 g, 2.5 mmol) in 15 cm^3 of water. The mixture was stirred at 60 °C for 2.5 h, whereupon it became a dark-brown solution. After the solution had been stood at room temperature for 1 d, the resulting dark-orange crystals (**1**(NO$_3$)$_2$·3.5H$_2$O) were collected by filtration. To this mother liquor was added 5 cm^3 of a saturated NaNO$_3$ solution, followed by standing at room temperature for 3 d. This second crop of the product was collected by filtration. Yield: 0.15 g (49%).

[Rh$_2$(aet)$_4$(crysta)]$^{2+}$ (2). Method A: *fac*(*S*)-[Rh(aet)$_3$] (0.30 g, 0.91 mmol) was dissolved in 10 cm^3 of 1 mol dm^{-3} HCl. To the yellow solution was added K$_2$Cr$_2$O$_7$ (0.047 g, 0.16 mmol). The mixture was stirred at room temperature for 15 min, whereupon it became a dark-orange solution. To this solution was added 1 cm^3 of a saturated NaCl solution, followed by standing at room temperature for 1 d. The resulting dark-orange crystals (**2**Cl$_2$·2H$_2$O) were collected by filtration, and one of the crystals was used for an X-ray structural analysis. Yield: 0.099 g (28%). Found: C, 18.52; H, 5.25; N, 10.65%. Calcd for [Rh$_2$(aet)$_4$(cysta)]Cl$_2$·2H$_2$O = C$_{12}$H$_{36}$N$_6$S$_6$Cl$_2$Rh$_2$·2H$_2$O: C, 18.73; H, 5.24; N, 10.92%.

Method B: To a suspension containing *fac*(*S*)-[Rh(aet)$_3$] (0.10 g, 0.30 mmol) in 2 cm^3 of water was added Ce(SO$_4$)$_2$·4H$_2$O (0.13 g, 0.31 mmol). After the mixture had been stirred at room temperature for 1 h, the resulting orange powder (**2** SO$_4$) was collected by filtration. The counter anion was exchanged by adding this powder into 5 cm^3 of a saturated NaNO$_3$ solution at 40 °C for 10 min. The resulting orange powder (**2**(NO$_3$)$_2$·2H$_2$O) was recrystallized from warm water by adding a few drops of a saturated NaNO$_3$ solution. Yield: 0.052 g (42%). Found: C, 17.36; H, 4.82; N, 13.55%. Calcd for [Rh$_2$(aet)$_4$(cysta)](NO$_3$)$_2$·2H$_2$O = C$_{12}$H$_{36}$N$_8$O$_6$S$_6$Rh$_2$·2H$_2$O: C, 17.52; H, 4.90; N, 13.62%.

Measurements. The electronic absorption spectra were recorded with a JASCO V-560 spectrophotometer. All of the measurements were carried out in aqueous solutions at room temperature. The elemental analyses (C, H, N) were performed by the Analysis Center of the University of Tsukuba. The infrared spectra were recorded as KBr disk with a JASCO FT/IR-550 spectrometer. The ^{13}C NMR spectra were recorded with a Bruker AM-500 NMR spectrometer in D$_2$O. The sodium 4,4-dimethyl-4-silapentane-1-sulfonate (DSS) was used as an internal reference. The molar conductances of the complexes were measured with a Horiba conductivity meter DS-14 in aqueous solutions at room temperature. Electrochemical measurements were made by the CV-1B apparatus (Biochemical Analytical Systems, Inc. (BAS)) using a glassy-carbon working electrode (BAS, GCE). An aqueous Ag/AgCl/NaCl (3 mol dm^{-3}) electrode (BAS, RE-1) and platinum wire were used as reference and auxiliary electrodes, respectively. Electrochemical experiments were conducted in a 0.1 mol dm^{-3} sodium sulfate aqueous solution as the supporting electrolyte and the complex concentrations of 1.0 mmol dm^{-3}.

Crystallography. Single crystals of **1**Cl$_2$·4H$_2$O and **2**Cl$_2$·2H$_2$O were used for data collection on a Rigaku RASA-7S four-circle diffractometer with graphite-monochromatized Mo $K\alpha$ radiation. The unit-cell parameters were determined by a least-squares refinement of 25 reflections ($14.8 < \theta < 15°$). The crystal data and experimental parameters are listed in Table 1. The intensity data were collected by the ω–2θ scan technique, and the scan rate varied from 1 to 5° min^{-1} (on ω). The intensities were corrected for Lorentz and polarization. An empirical absorption correction based on a series of Ψ scans was applied. The independent reflections with $I_0 > 1.5\sigma(I_0)$ were used for structure determinations. The positions of the Ir or Rh and other atoms were determined by a direct method. The difference Fourier maps based on these atomic positions revealed some remaining non-hydrogen atoms. The structures were refined by a full-matrix least-squares refinement on F of the positional parameters and the anisotropic thermal parameters of the non-hydrogen atoms in **1**Cl$_2$·4H$_2$O or **2**Cl$_2$·2H$_2$O. The hydrogen atoms on the aet ligands were fixed by the geometrical and thermal constrains (C–H = N–H = 0.95 Å and $U = 1.3U$(C, N)). All of the calculations were performed on Indigo II computer using teXsan.[18] The final atomic coordinates for non-hydrogen atoms are given in Tables 2 and 3.[19]

Results and Discussion

Stereochemistry. X-Ray structural analysis for each of the dark orange crystals (**1**Cl$_2$·4H$_2$O and **2**Cl$_2$·2H$_2$O) revealed the presence of a discrete complex cation, two chloride anions, and some water molecules.[20] Perspective drawings of the entire complex cations **1** and **2** are given in Figs. 1 and 2, respectively. The selected bond distances and angles are listed in Table 4. As shown in Figs. 1 and 2, the complex cation **1** is isostructural with **2**, that is, **1** and **2** consist of two approximately octahedral *fac*(*S*)-[M(aet)$_3$] (M = Ir, Rh) units, which are linked by a sulfur-sulfur bond (S(1)–S(1)* = 2.158(3) Å for **1**; 2.147(1) Å for **2**). In both of the

Table 1. Crystal Data of $[Ir_2(aet)_4(cysta)]Cl_2\cdot 4H_2O$ ($\mathbf{1}Cl_2\cdot 4H_2O$) and $[Rh_2(aet)_4(cysta)]$-$Cl_2\cdot 2H_2O$ ($\mathbf{2}Cl_2\cdot 2H_2O$)

	$\mathbf{1}Cl_2\cdot 4H_2O$	$\mathbf{2}Cl_2\cdot 2H_2O$
Formula	$C_{12}H_{44}N_6O_4S_6Cl_2Ir_2$	$C_{12}H_{40}N_6O_2S_6Cl_2Rh_2$
Fw	984.22	769.56
Cryst dimens/mm	$0.50\times 0.25\times 0.23$	$0.45\times 0.40\times 0.08$
Space group	$P2_1/a$ (No. 14)	$P2_1/c$ (No. 14)
a/Å	12.427(2)	11.788(2)
b/Å	8.879(1)	8.485(1)
c/Å	13.387(1)	14.800(2)
β/deg	91.947(10)	112.980(9)
V/Å^3	1476.3(3)	1362.9(3)
Z	2	2
D_{calcd}/g cm^{-3}	2.214	1.875
μ/cm^{-1}	9.665	1.886
Transm factor	0.46—1.00	0.71—1.00
Scan type	ω–2θ	ω–2θ
θ range/deg	55.0	55.0
No. of reflcns measd	3619	3342
No. of reflcns used	3159	2872
No. of variables used	146	137
R (R_w)	0.031 (0.052)	0.023 (0.048)
GOF	1.464	1.348

Table 2. Final Atomic Coordinates and Equivalent Isotropic Thermal Parameters (U_{eq}/Å^2)[a] for $[Ir_2(aet)_4(cysta)]$-$Cl_2\cdot 4H_2O$ ($\mathbf{1}Cl_2\cdot 4H_2O$)

Atom	x	y	z	U_{eq}
Ir	0.50129(1)	0.11181(2)	0.80269(1)	0.01987(8)
S(1)	0.4475(1)	0.0784(2)	0.96063(10)	0.0242(3)
S(2)	0.6251(1)	0.2955(2)	0.8549(1)	0.0284(3)
S(3)	0.6280(1)	−0.0839(2)	0.8021(1)	0.0312(3)
N(1)	0.3825(4)	−0.0534(6)	0.7591(4)	0.031(1)
N(2)	0.3896(4)	0.2948(6)	0.7892(4)	0.029(1)
N(3)	0.5466(4)	0.1482(6)	0.6550(4)	0.029(1)
C(1)	0.3336(5)	−0.0491(8)	0.9374(5)	0.035(2)
C(2)	0.3532(5)	−0.1455(7)	0.8486(5)	0.038(2)
C(3)	0.5422(6)	0.4616(7)	0.8311(6)	0.043(2)
C(4)	0.4260(5)	0.4285(7)	0.8474(5)	0.039(2)
C(5)	0.6800(5)	−0.0543(8)	0.6769(5)	0.035(2)
C(6)	0.5951(5)	0.0124(7)	0.6083(4)	0.032(1)
Cl	0.6737(1)	0.4834(2)	0.5891(1)	0.0491(4)
O(1w)	0.4393(5)	−0.3169(8)	0.6125(5)	0.068(2)
O(2w)	0.3465(4)	0.2675(6)	0.5724(4)	0.051(1)

a) U_{eq} denotes the equivalent isotropic temperature factors, $U_{eq}=(1/3)\sum_i\sum_j U_{ij}a_i^*a_j^*\boldsymbol{a}_i\cdot\boldsymbol{a}_j$.

Table 3. Final Atomic Coordinates and Equivalent Isotropic Thermal Parameters (U_{eq}/Å^2)[a] for $[Rh_2(aet)_4(cysta)]$-$Cl_2\cdot 2H_2O$ ($\mathbf{2}Cl_2\cdot 2H_2O$)

Atom	x	y	z	U_{eq}
Rh	0.80566(2)	0.35584(2)	0.03946(1)	0.01783(8)
S(1)	0.92268(5)	0.54947(7)	0.01120(4)	0.0219(1)
S(2)	0.92558(7)	0.35268(7)	0.20713(5)	0.0283(2)
S(3)	0.91528(7)	0.15076(7)	0.00878(6)	0.0259(2)
N(1)	0.6966(2)	0.3688(2)	−0.1154(2)	0.0254(5)
N(2)	0.6992(2)	0.5337(3)	0.0765(1)	0.0259(5)
N(3)	0.6950(2)	0.1776(3)	0.0591(2)	0.0260(5)
C(1)	0.8280(2)	0.5900(3)	−0.1169(2)	0.0284(6)
C(2)	0.7662(2)	0.4415(3)	−0.1684(2)	0.0291(6)
C(3)	0.8341(3)	0.4890(4)	0.2478(2)	0.0366(7)
C(4)	0.7742(3)	0.6122(3)	0.1720(2)	0.0337(7)
C(5)	0.8212(3)	−0.0134(3)	0.0164(2)	0.0360(7)
C(6)	0.7609(3)	0.0248(3)	0.0878(2)	0.0345(7)
Cl	0.50951(7)	0.68677(10)	−0.14360(6)	0.0427(2)
O(1w)	0.5126(3)	0.0723(3)	−0.1438(2)	0.0615(8)

a) U_{eq} denotes the equivalent isotropic temperature factors, $U_{eq}=(1/3)\sum_i\sum_j U_{ij}a_i^*a_j^*\boldsymbol{a}_i\cdot\boldsymbol{a}_j$.

complexes **1** and **2**, a half of the complex cations and two chloride anions are crystallographically independent in the unit-cell. This implies that all complex cations are divalent. This is compatible with the observed molar conductivity in water of 208 S cm^2 mol^{-1} for **1** and 227 S cm^2 mol^{-1} for **2**, which are in agreement with those of the 1 : 2 electrolytes, $[Pt(bpy)\{Ni(aet)_2L\}]^{2+}$ (L = $(H_2O)_2$ or bpy; bpy = 2,2′-bipyridine) (216—228 S cm^2 mol^{-1}).[21] From these results and the formal charge of the coordinated ligands, it is reasonable to assume that the oxidations occur only at one coordinated thiolato group in the *fac*(*S*)-[M(aet)$_3$] units to form the disulfide bond, while the Ir or Rh atom retains the +3 oxidation state.

Considering the absolute configurations of the two octahedral *fac*(*S*)-[M(aet)$_3$] units (Δ and Λ) and the two asymmetric disulfide sulfur atoms (R and S), ten isomers are possible for $[M_2(aet)_4(cysta)]^{2+}$.[22] Both of the crystals $\mathbf{1}Cl_2\cdot 4H_2O$ and $\mathbf{2}Cl_2\cdot 2H_2O$ contain only meso form with the $\Delta_R\Lambda_S$ configuration, as shown in Figs. 1 and 2. Furthermore, when the reaction solutions for $[M_2(aet)_4(cysta)]^{2+}$ were chromatographed on an SP-Sephadex C-25 column, only one orange band was eluted with a 0.15 mol dm^{-3} NaCl solution. Molecular model examinations reveal that the racemic

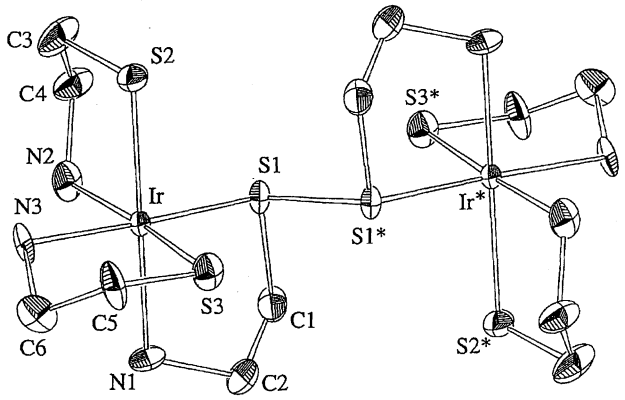

Fig. 1. Perspective view of $\Delta_R\Lambda_S$-$[Ir_2(aet)_4(cysta)]^{2+}$ (**1**) with the atomic labeling scheme.

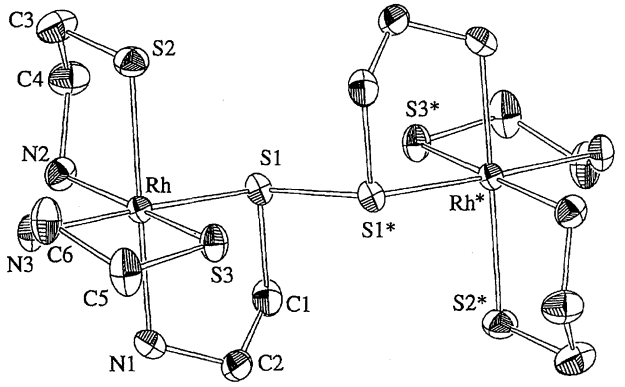

Fig. 2. Perspective view of $\Delta_R\Lambda_S$-$[Rh_2(aet)_4(cysta)]^{2+}$ (**2**) with the atomic labeling scheme.

form exhibit a larger non-bonding interaction between two $[M(aet)_3]$ units than that of the meso form. Accordingly, these facts seem to imply that the $\Delta_R\Lambda_S$ isomer is selectively formed by the oxidation reactions for the present disulfide complexes.

The Ir–N(3) distance (2.099(5) Å) in $\Delta_R\Lambda_S$-$[Ir_2(aet)_4(cysta)]^{2+}$ is shorter than the Ir–N(1) (2.148(5) Å) and Ir–N(2) (2.141(5) Å) distances. A similar trend was also observed for the corresponding Rh complex **2** (Table 4). The N(3) atom occupies the *trans* position to the disulfide sulfur atom, while the N(1) and N(2) atoms take the *trans* positions to the thiolato sulfur atoms. Therefore, these seem to depend on the *trans* influence for the thiolato sulfur atom. This is compatible with the results that the thiolato sulfur atom in $[Co(aet)(en)_2]^{2+}$ exerts a significant trans influence,[23] while the disulfide sulfur atom in $[Co\{NH_2CH_2CH_2S(SCH_2CH_3)\}(en)_2]^{3+}$ does not.[24] On the other hand, the Co–S distance (2.272(2) Å) in $[Co\{NH_2CH_2CH_2S(SCH_2CH_3)\}(en)_2]^{3+}$ is longer than that (2.226(6) Å) in $[Co(aet)(en)_2]^{2+}$.[23,24] However, the M–S(1) distances (for M = Ir, 2.258(1) Å; Rh, 2.2865(6) Å) are shorter than the M–S(2) and M–S(3) distances (Ir, av. 2.339(1) Å; Rh, av. 2.3217(7) Å). Accordingly, this suggests that the disulfide sulfur atoms in $[M_2(aet)_4(cysta)]^{2+}$ are bound to the Ir or Rh atom more strongly than to the Co atom. The stronger M–S bonding for the Ir and Rh atoms than the Co atom would be related to the longer sulfur–sulfur distances of the disulfide bond, that is, the S(1)–S(1)* distances (M = Ir, 2.158(3) Å; Rh, 2.147(1) Å), whose distance (2.142(5) Å) was also observed for the S-bridged octanuclear complex, $[Cu_4\{Rh(aet)_3\}_2\{Rh_2(aet)_4(cysta)\}]^{6+}$,[7] are significantly longer than that (2.033(3) Å) of $[Co\{NH_2CH_2CH_2S(SCH_2CH_3)\}(en)_2]^{3+}$.[24]

Table 4. Selected Bond Distances (Å) and Angles (deg.) for $[Ir_2(aet)_4(cysta)]^{2+}$ and $[Rh_2(aet)_4(cysta)]^{2+}$

$[Ir_2(aet)_4(cysta)]^{2+}$ (**1**)		$[Rh_2(aet)_4(cysta)]^{2+}$ (**2**)	
Ir–S(1)	2.258(1)	Rh–S(1)	2.2865(6)
Ir–S(2)	2.333(1)	Rh–S(2)	2.3276(7)
Ir–S(3)	2.345(1)	Rh–S(3)	2.3157(6)
Ir–N(1)	2.148(5)	Rh–N(1)	2.149(2)
Ir–N(2)	2.141(5)	Rh–N(2)	2.166(2)
Ir–N(3)	2.099(5)	Rh–N(3)	2.090(2)
S(1)–S(1)*	2.158(3)	S(1)–S(1)*	2.147(1)
S(1)–Ir–S(2)	91.42(5)	S(1)–Rh–S(2)	92.56(2)
S(1)–Ir–S(3)	97.22(5)	S(1)–Rh–S(3)	94.67(2)
S(1)–Ir–N(1)	86.7(1)	S(1)–Rh–N(1)	85.42(6)
S(1)–Ir–N(2)	88.1(1)	S(1)–Rh–N(2)	89.78(6)
S(1)–Ir–N(3)	177.9(1)	S(1)–Rh–N(3)	177.67(6)
S(2)–Ir–S(3)	94.76(6)	S(2)–Rh–S(3)	92.71(3)
S(2)–Ir–N(1)	177.5(1)	S(2)–Rh–N(1)	177.66(6)
S(2)–Ir–N(2)	85.1(1)	S(2)–Rh–N(2)	84.76(6)
S(2)–Ir–N(3)	88.8(1)	S(2)–Rh–N(3)	89.73(7)
S(3)–Ir–N(1)	87.0(1)	S(3)–Rh–N(1)	88.65(6)
S(3)–Ir–N(2)	174.7(1)	S(3)–Rh–N(2)	174.97(6)
S(3)–Ir–N(3)	84.8(1)	S(3)–Rh–N(3)	84.82(7)
N(1)–Ir–N(2)	93.3(2)	N(1)–Rh–N(2)	94.03(8)
N(1)–Ir–N(3)	93.1(2)	N(1)–Rh–N(3)	92.29(9)
N(2)–Ir–N(3)	89.9(2)	N(2)–Rh–N(3)	90.81(9)
Ir–S(1)–S(1)*	110.42(9)	Rh–S(1)–S(1)*	110.88(4)

Most of the bond distances around the Ir atom for $\Delta_R\Lambda_S$-$[Ir_2(aet)_4(cysta)]^{2+}$ are reasonably larger than those around the Rh atom for $\Delta_R\Lambda_S$-$[Rh_2(aet)_4(cysta)]^{2+}$, considering the covalent radii of the Ir and Rh metals (Table 4). However, the Ir–S(1) (2.258(1) Å) and Ir–N(1) (2.148(5) Å) distances of the cysta ligand for $\Delta_R\Lambda_S$-$[Ir_2(aet)_4(cysta)]^{2+}$ are shorter than those (Rh–S(1), 2.2865(6); Rh–N(1), 2.149(2) Å) for the corresponding Rh complex (**2**). The bond angles around the Ir atom for **1** are quite similar to those of the Rh atoms for **2**, except for the S(1)–M–S(3) (Ir, 97.22(5)°; Rh, 94.67(2)°) and S(2)–M–S(3) (Ir, 94.76(6)°; Rh, 92.71(3)°) angles. These suggest that the geometry around the disulfide sulfur atom in $\Delta_R\Lambda_S$-$[Ir_2(aet)_4(cysta)]^{2+}$ is affected by the S–S bond (Table 4), and its sulfur atom is bound to the Ir atom more strongly than that in the corresponding Rh complex to the Rh atom. As shown in Figs. 1 and 2, furthermore, S(3)–N(3) chelate rings are the parallel conformations (λ for Δ_R; δ for Λ_S) on pseudo-C_3 axis for $\Delta_R\Lambda_S$-$[Ir_2(aet)_4(cysta)]^{2+}$, while the oblique conformations (δ for Δ_R; λ for Λ_S) for the Rh complex, although all of the other chelate rings take only the oblique conformations of on the pseudo-C_3 axis. These seem to indicate that the oblique conformations are more favorable in $\Delta_R\Lambda_S$-$[M_2(aet)_4(cysta)]^{2+}$ than the parallel ones.

Characterization. The ^{13}C NMR chemical shifts of $\Delta_R\Lambda_S$-$[M_2(aet)_4(cysta)]^{2+}$ (M = Ir^{III} (**1**), Rh^{III} (**2**)) are listed in Table 5, together with some other related polynuclear complexes. Each of **1** and **2** exhibits six signals due to the twelve methylene carbon atoms of the aet and cysta ligands because of the meso form. They are divided into three kinds of groups, that is, two signals (δ = 52—55) at the lower field, two signals (δ = 29—34) at the higher field, and two signals (δ = 45—48) at the middle field. The trinuclear $[Co\{M(aet)_3\}_2]^{3+}$ complexes, which also have the twelve methylene carbon atoms of the aet ligands, exhibit only two signals due to two kinds of methylene carbon atoms, and it is assignable that the signal (δ = 49—52) at the lower field is due to the carbon atoms adjacent to the amino group and the signal (δ = 33—35) at the higher field due to those to the bridging sulfur atoms.[1a,2a] Similar trends were also observed for the T-cage-type polynuclear complexes (δ = 51—53 and 33—35; Table 5).[4c,5b] On the other hand, the ^{13}C NMR spectra of $[Cu_4\{M(aet)_3\}_2\{M_2(aet)_4(cysta)\}]^{6+}$ (M = Ir^{III}, Rh^{III}), which contain not only the aet ligands, but also the cysta ligand with the coordinated disulfide, exhibit several additional signals (δ = 43—49) at middle field to the two kinds of groups (δ = 51—54 and 34—37). These facts suggest that the signals due to methylene carbon atoms of the cysta ligand with the disulfide bond would appear in this middle field region, and the other signals at the lower and higher fields are also due to the methylene carbon atoms for the aet ligands. It is noted in the present dinuclear complexes, $[Co\{M(aet)_3\}_2]^{3+}$,[1a,2a] $[\{M(aet)_3\}_4M_4O]^{6+}$,[4c,5b] and $[Cu_4\{M(aet)_3\}_2\{M_2(aet)_4(cysta)\}]^{6+}$ [7] that the chemical shifts of the aet ligand in the Ir complexes are more separated than those of the Rh complexes. Taking account of these ^{13}C NMR spectral behavior, the molar conductivity and the absorption spectra (vide infra), which changes little at least for several hours, accordingly, it seems to be indicated that $\Delta_R\Lambda_S$-$[M_2(aet)_4(cysta)]^{2+}$ are fairly stable in solution, and the disulfide-bridged dinuclear structure observed in crystals are retained in the aqueous solution.

The absorption spectra of $[M_2(aet)_4(cysta)]^{2+}$ (M = Ir^{III} (**1**), Rh^{III} (**2**)), are shown in Fig. 3, and their data are summarized in Table 6, together with the corresponding *fac*(*S*)-$[M(L\text{-cys-}N,S)_3]^{3-}$ and/or *fac*(*S*)-$[M(aet)_3]$. The absorption spectrum of $[Ir_2(aet)_4(cysta)]^{2+}$ is quite similar to that of 2 mol of *fac*(*S*)-$[Ir(L\text{-cys-}N,S)_3]^{3-}$ at the high energy region,

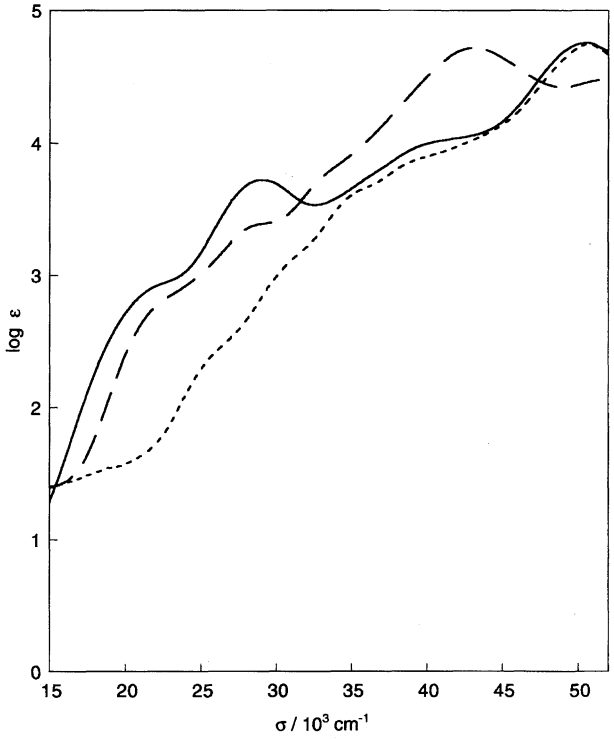

Fig. 3. Absorption spectra of $[M_2(aet)_4(cysta)]^{2+}$(M = Ir, —; Rh – – –), and *fac*(*S*)-$[Ir(L\text{-cys-}N,S)_3]^{3-}$×2 (- - -).

Table 5. ^{13}C NMR Chemical Shifts[a] of $[M_2(aet)_4(cysta)]^{2+}$ and Its Related Complexes

Complexes	aet NH_2–CH_2	cysta NH_2–CH_2	cysta S–CH_2	aet S–CH_2
$\Delta_R\Lambda_S$-$[Ir_2(aet)_4(cysta)]^{2+}$ (**1**)	55.11	47.66	45.11	32.36
	54.11			29.77
$\Delta_R\Lambda_S$-$[Rh_2(aet)_4(cysta)]^{2+}$ (**2**)	54.85	46.20	45.50	33.83
	52.33			31.14
meso-$[Co\{Ir(aet)_3\}_2]^{3+}$ [b]	51.64			33.74
meso-$[Co\{Rh(aet)_3\}_2]^{3+}$ [c]	49.89			34.40
$[\{Ir(aet)_3\}_4Zn_4O]^{6+}$ [d]	52.69			33.36
$[\{Rh(aet)_3\}_4Zn_4O]^{6+}$ [e]	51.20			33.86
$[Cu_4\{Ir(aet)_3\}_2\{Ir_2(aet)_4(cysta)\}]^{6+}$ [f,g]	54.09	48.51	44.20	35.72
	53.53	47.14	43.39	35.06
	53.04			34.55
	52.88			
$[Cu_4\{Rh(aet)_3\}_2\{Rh_2(aet)_4(cysta)\}^{6+}$ [f,g]	53.76	46.96	45.06	36.79
	51.68		44.63	35.93
	51.24			
	51.07			

a) In ppm from DSS. b) Ref. 2a. c) Ref. 1a. d) Ref. 5b. e) Ref. 4c. f) Ref. 7. g) These complexes have three different types of sulfur atoms, μ_2- and μ_3-thiolato and disulfide. Accordingly, assignments of signals are not clearly.

Table 6. Electronic Absorption Spectral Data of $[M_2(aet)_4(cysta)]^{2+}$

Complexes	Absorption maxima $\sigma/10^3$ cm^{-1} ($\log \varepsilon$/mol^{-1} dm^3 cm^{-1})		
$[Ir_2(aet)_4(cysta)]^{2+}$ (**1**)	22.0 (2.9 sh[a)])	29.07 (3.72)	35.5 (3.7 sh)
	40.8 (4.0 sh)	50.63 (4.76)	
$[Rh_2(aet)_4(cysta)]^{2+}$ (**2**)	22.4 (2.8 sh)	29.1 (3.4 sh)	33.9 (3.8 sh)
	43.10 (4.72)		
fac(*S*)-$[Ir(L\text{-}cys\text{-}N,S)_3]^{3-}$ [b)]	27.8 (3.3 sh)	31.7 (2.9 sh)	36.0 (3.4 sh)
	41.3 (3.7 sh)	50.76 (4.45)	
fac(*S*)-$[Rh(aet)_3]$ [c)]	26.3 (2.9 sh)	30.03 (3.10)	44.05 (4.59)
fac(*S*)-$[Rh(L\text{-}cys\text{-}N,S)_3]^{3-}$ [c)]	26.3 (2.9 sh)	29.59 (3.05)	43.48 (4.61)

a) sh denotes a shoulder. b) Ref. 2a. c) Ref. 4c.

which exhibit two spin-allowed d–d transition bands at ca. 32—41$\times 10^3$ cm^{-1} and the sulfur-to-iridium charge transfer band at ca. 50$\times 10^3$ cm^{-1} (Fig. 3 and Table 6).[2a)] A similar trend was observed for the corresponding Rh complexes (25—32$\times 10^3$ cm^{-1} for d–d transition; ca. 43$\times 10^3$ cm^{-1} for sulfur-to-rhodium charge transfer transition; Fig. 3 and Table 6).[4c)] These absorption spectral behaviors were also observed for the T-cage-type polynuclear complexes,[3—6)] in which the Zn^{2+}, Cd^{2+}, and Hg^{2+} metals take the d^{10} electron states and their complexes are almost colorless. In contrast with these polynuclear complexes, the present dinuclear complexes $[M_2(aet)_4(cysta)]^{2+}$ are orange, and their absorption bands are intensified in the visible and near-ultraviolet regions (15—32$\times 10^3$ cm^{-1} for Ir complex; 15—25$\times 10^3$ cm^{-1} for Rh complex). This seems to depend on the fact that the thiolato sulfur atoms, which coordinated to the Ir or Rh atom, are oxidized to form the disulfide bond. The absorption bands of $[Rh_2(aet)_4(cysta)]^{2+}$ in this region are significantly smaller intensification than the corresponding Ir complex (Fig. 3 and Table 6). Considering the M–S distances for the disulfide and the thiolate groups, which are determined by the crystal structures analyses, it seems that the intensified bands in the visible and near-ultraviolet regions highly depend upon the shorter M–S distances than the usual ones and would be dominated by the sulfur-to-metal charge transfer transitions.

As shown in Fig. 4, the infrared spectral pattern of $[M_2(aet)_4(cysta)]^{2+}$ (M = Ir^{III}, Rh^{III}) and *fac*(*S*)-$[M(aet)_3]$ coincide well each other in the region of 400—1000 cm^{-1}, although slight shifts are observed. In the region near 570 cm^{-1}, however, the characteristic bands are appeared in $[M_2(aet)_4(cysta)]^{2+}$ but not in *fac*(*S*)-$[M(aet)_3]$. No significant spectral difference of the dinuclear complexes are caused by the difference of the Ir(III) and Rh(III) ions. Accordingly, it can be assigned that the characteristic bands at ca. 570 cm^{-1} are due to disulfide bond coordinated to the metal ions.

Electrochemical studies were performed for $[M_2(aet)_4(cysta)]^{2+}$ (M = Ir^{III} (**1**), Rh^{III} (**2**)) complexes in 0.1 mol dm^{-3} sodium sulfate aqueous solutions. As shown in Fig. 5, the cyclic voltammograms at a glassy-carbon electrode for both **1** and **2** display an irreversible oxidation waves at a positive potential region and an irreversible reduction wave at

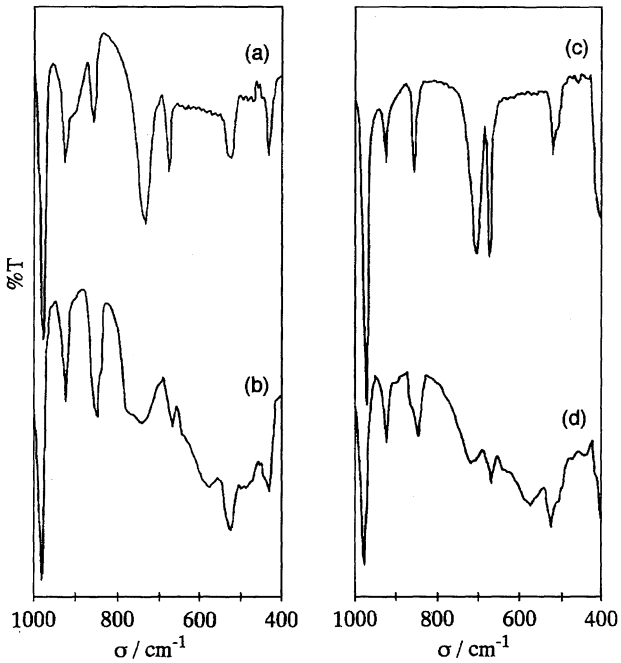

Fig. 4. Infrared spectra of (a) *fac*(*S*)-$[Ir(aet)_3]$, (b) $[Ir_2(aet)_4(cysta)]^{2+}$, (c) *fac*(*S*)-$[Rh(aet)_3]$, and (d) $[Rh_2(aet)_4(cysta)]^{2+}$.

a negative potential region. It seems to be indicated that the irreversible oxidation wave at (E_{pa} = +0.60 V) for **1** involves the terminal Ir(III)/Ir(IV) oxidation process, because the redox couples for the Ir(III)/Ir(IV) redox process of $[M\{Ir(aet)_3\}_2]^{3+}$ are appeared at a similar positive region (M = Cr, $E^{o\prime}$ = +0.64 V; Co, +0.73 V).[2)] Similarly, the irreversible oxidation wave (E_{pa} = +0.77 V) for **2** would involve the terminal Rh(III)/Rh(IV) oxidation process, because the redox couples are appeared at a similar positive region to the corresponding Rh complexes (both of Cr and Co, $E^{o\prime}$ = +1.01 V).[2)] These suggests, therefore, that **1** is easily oxidized than **2**.

The irreversible reduction waves (E_{pc} = −0.63 V) for **1** appear at almost the same potential as that (E_{pc} = −0.58 V) for **2**. Since it has been known that the Ir(III)/Ir(II) and Rh(III)/Rh(II) redox process does not occur in the potential region of +1.1——1.1 V for $[M\{M'(aet)_3\}_2]^{3+}$ (M = Cr^{III}, Co^{III}; M′ = Ir^{III}, Rh^{III}),[2)] the irreversible reduction waves have

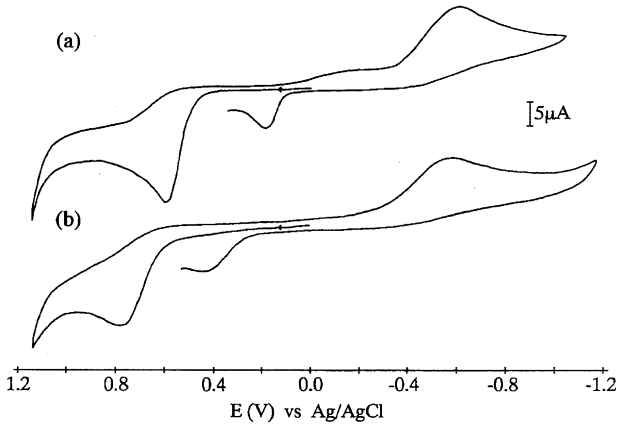

Fig. 5. Cyclic voltammograms of (a) $[Ir_2(aet)_4(cysta)]^{2+}$ and (b) $[Rh_2(aet)_4(cysta)]^{2+}$; scan rate 100 mV s^{-1}; in 0.1 mol dm^{-3} Na_2SO_4 solution.

probably influence on the cleavage of the disulfide bond. In fact, the addition of reducing agent, such as $NaBH_4$, to the present dinuclear complexes gave the mononuclear thiolato complexes, *fac*(*S*)-[M(aet)$_3$]. The irreversible oxidation waves (E_{pa} = +0.19 V for **1** and +0.44 V for **2**) are not observed unless going through the reduction scans. This suggests that the dinuclear complexes are decomposed by the reduction process and the created species with the metal ions might be oxidized by the oxidation process. Since only irreversible waves are observed about both of reduction and oxidation processes, it seems to be indicated that the dinuclear structures no longer exist in the process.

Reactivity. The reaction of *fac*(*S*)-[Ir(aet)$_3$] with acid (1 mol dm^{-3} HCl solution) in water gave dinuclear complexes, $\Delta_R\Lambda_S$-$[Ir_2(aet)_4(cysta)]^{2+}$. In this reaction, the oxidation is proceeded by the acid. This is supported by the results that the same dinuclear complexes were also produced by the reactions of *fac*(*S*)-[Ir(aet)$_3$] with 0.15 mol dm^{-3} HNO_3 solution, $Ce(SO_4)_2{\cdot}4H_2O$ or $Cr(NO_3)_3{\cdot}9H_2O$. In contrast to the Ir dinuclear complexes, $[Rh_2(aet)_4(cysta)]^{2+}$ are hardly formed by a procedure similar to that for the acid solution (1 mol dm^{-3} HCl), using *fac*(*S*)-[Rh(aet)$_3$] instead of *fac*(*S*)-[Ir(aet)$_3$]. In the ^{13}C NMR spectral measurements, the treatment of *fac*(*S*)-[Rh(aet)$_3$] with 1 mol dm^{-3} DCl showed only two signals due to the aet ligands, and no signal for $[Rh_2(aet)_4(cysta)]^{2+}$ is shown even when the sample was allowed to stand for a week at room temperature. When the reaction mixture was heated, the ^{13}C NMR signals appeared at the field of free ligands. A similar dissociation of the ligands was not observed in the case of *fac*(*S*)-[Ir(aet)$_3$], and the *fac*(*S*)-[Ir(aet)$_3$] units in the dinuclear complex are relatively stable to heat and oxidized by the acid. These seem to indicate that the Rh–S bonds in acid solution are snapped before forming the disulfide bonds. Further, the reaction of *fac*(*S*)-[Ir(aet)$_3$] with Cr^{3+} was accompanied by the dinuclear Ir complex, but by the unidentified Rh complex.[2b] $[Rh_2(aet)_4(cysta)]^{2+}$ are formed by the reaction with a strong oxidizing agent of $K_2Cr_2O_7$ or $Ce(SO_4)_2$. This coincides well with the fact that *fac*(*S*)-[Ir(aet)$_3$] would be oxidized more easily than *fac*(*S*)-[Rh(aet)$_3$]. Accordingly, these facts seem to indicate that the Rh–S bonds in the *fac*(*S*)-[Rh(aet)$_3$] units are weaker than the corresponding Ir–S bonds and then *fac*(*S*)-[Ir(aet)$_3$] would be oxidized more easily than *fac*(*S*)-[Rh(aet)$_3$] to form the disulfide bonds.

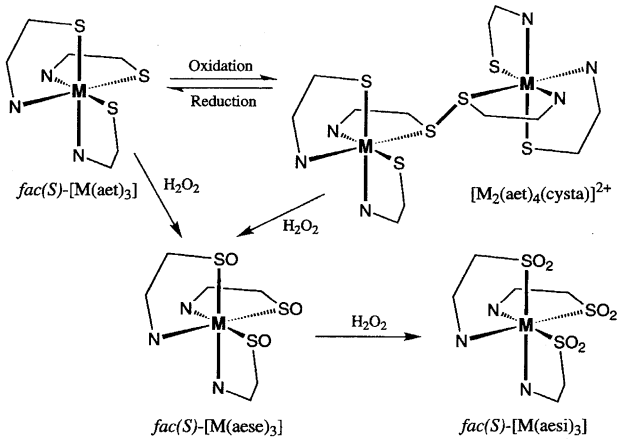

Scheme 1.

In the present work, the novel dinuclear complexes, $[M_2(aet)_4(cysta)]^{2+}$, with a coordinated bridging disulfide bond are formed by the oxidation reaction for the first time (Scheme 1). When a base, such as NaOH or $NaBH_4$, is added to the aqueous solution of $[M_2(aet)_4(cysta)]^{2+}$, the white or yellow suspension is appeared immediately, from which *fac*(*S*)-[M(aet)$_3$] are precipitated in a quantitative yield. When the dinuclear complexes are further oxidized using excess H_2O_2, the mononuclear sulfinato complexes, *fac*(*S*)-[M(aesi)$_3$] are obtained (Scheme 1). This oxidation reaction reveals that the disulfide bonds are cleaved. Similar sulfinato complexes are also formed by the direct oxidation using H_2O_2 of the thiolato complexes (Scheme 1).[10,11,25] Taking account of the M–S and S–S distances for the disulfide bonds of $[M_2(aet)_4(cysta)]^{2+}$ in the crystal structure analysis, it is reasonable to assume that the disulfide bonds are cleaved, because the dinuclear structure is stereochemically labilized by the oxygen atoms which are bounded to thiolato sulfur atoms due to oxidation reaction. Namely, the coordinated disulfide in the present complexes is cleaved by not only reduction, but also oxidation, which does not involve the M–S bond cleavage.

This work was supported by Grant-in-Aid for Scientific Research No. 07454172 from the Ministry of Education, Science, Sports and Culture.

References

1) a) T. Konno, S. Aizawa, K. Okamoto, and J. Hidaka, *Bull. Chem. Soc. Jpn.*, **63**, 792 (1990); b) T. Konno, K. Okamoto, and J. Hidaka, *Acta Crystallogr., Sect. C*, **C49**, 222 (1993); c) T. Konno and K. Okamoto, *Bull. Chem. Soc. Jpn.*, **68**, 610 (1995).

2) a) T. Konno, K. Nakamura, K. Okamoto, and J. Hidaka, *Bull. Chem. Soc. Jpn.*, **66**, 2582 (1993); b) Y. Miyashita, N. Sakagami, Y. Yamada, T. Konno, J. Hidaka, and K. Okamoto, *Bull. Chem. Soc. Jpn.*, **71**, 661 (1998).

3) T. Konno, T. Nagashio, K. Okamoto, and J. Hidaka, *Inorg. Chem.*, **31**, 1160 (1992).

4) a) T. Konno, K. Okamoto, and J. Hidaka, *Chem. Lett.*, **1990**, 1043; b) T. Konno, K. Okamoto, and J. Hidaka, *Bull. Chem. Soc. Jpn.*, **67**, 101 (1994); c) T. Konno, K. Okamoto, and J. Hidaka, *Inorg. Chem.*, **33**, 538 (1994); d) T. Konno, Y. Kageyama, and K. Okamoto, *Bull. Chem. Soc. Jpn.*, **67**, 1957 (1994); e) Y. Kageyama, T. Konno, K. Okamoto, and J. Hidaka, *Inorg. Chim. Acta*, **239**, 19 (1995).

5) a) T. Konno, K. Okamoto, and J. Hidaka, *Inorg. Chem.*, **30**, 2253 (1991); b) K. Okamoto, T. Konno, and J. Hidaka, *J. Chem. Soc., Dalton Trans.*, **1994**, 533.

6) a) K. Okamoto, T. Konno, Y. Kageyama, and J. Hidaka, *Chem. Lett.*, **1992**, 1105; b) K. Okamoto, Y. Kageyama, and T. Konno, *Bull. Chem. Soc. Jpn.*, **68**, 2573 (1995).

7) T. Konno, K. Okamoto, and J. Hidaka, *Inorg. Chem.*, **31**, 3875 (1992).

8) T. Konno, C. Sasaki, and K. Okamoto, *Chem. Lett.*, **1996**, 977.

9) T. Konno and K. Okamoto, *Inorg. Chem.*, **36**, 1403 (1997).

10) a) M. Kita, K. Yamanari, and Y. Shimura, *Chem. Lett.*, **1980**, 275; b) M. Kita, K. Yamanari, K. Kitahara, and Y. Shimura, *Bull. Chem. Soc. Jpn.*, **54**, 2995 (1981).

11) M. Kita, K. Yamanari, and Y. Shimura, *Bull. Chem. Soc. Jpn.*, **56**, 3272 (1983).

12) E. Deutsch, M. J. Root, and D. L. Nosco, *Adv. Inorg. Bioinorg. Mech.*, **1**, 269 (1982).

13) P. J. Blower and J. R. Dilworth, *Coord. Chem. Rev.*, **76**, 121 (1987).

14) M. Woods, J. Karbwang, J. C. Sullivan, and E. Deutsch, *Inorg. Chem.*, **15**, 1678 (1976).

15) J. D. Lydon, R. C. Elder, and E. Deutsch, *Inorg. Chem.*, **21**, 3186 (1982).

16) M. J. Heeg, E. L. Blinn, and E. Deutsch, *Inorg. Chem.*, **24**, 1118 (1985).

17) T. Konno, Y. Miyashita, and K. Okamoto, *Chem. Lett.*, **1997**, 85.

18) "teXsan. Molecular Structure Corporation. Single Crystal Structure Analysis Software. Version 1.8," MSC, 3200 Research Forest Drive, The Woodlands, TX 77381, USA (1997).

19) Lists of structure factors, hydrogen atoms coordinates, bond distances and angles, and anisotropic thermal parameters for non-hydrogen atoms are deposited as Document No. 71045 at the Office of the Editor of Bull. Chem. Soc. Jpn.

20) Although X-ray data for the tetrafluoroborate salt of the complex **1** has been reported as the preliminary result,[17] the data for the chloride salt were used in this work because of definite comparison with the Rh complex **2**.

21) T. Konno, Y. Yoshinari, and K. Okamoto, *Chem. Lett.*, **1995**, 989.

22) The possible isomers are $\Delta_S\Delta_S$, $\Delta_S\Delta_R$, $\Delta_R\Delta_R$, $\Delta_S\Lambda_S$, $\Delta_S\Lambda_R$, $\Delta_R\Lambda_S$, $\Delta_R\Lambda_R$, $\Lambda_S\Lambda_S$, $\Lambda_S\Lambda_R$, and $\Lambda_R\Lambda_R$.

23) R. C. Elder, L. R. Florian, R. E. Lake, and A. M. Yacynych, *Inorg. Chem.*, **12**, 2690 (1973).

24) D. L. Nosco, R. C. Elder, and E. Deutsch, *Inorg. Chem.*, **19**, 2545 (1980).

25) Anal. Found: C, 13.61; H, 3.75; N, 7.94%. Calcd for $[Ir(aesi)_3]\cdot 0.75H_2O$ = $C_6H_{18}N_3O_6S_3Ir\cdot 0.75H_2O$: C, 13.59; H, 3.71; N, 7.93%. Found: C, 16.26; H, 4.47; N, 9.53%. Calcd for $[Rh(aesi)_3]\cdot 0.75H_2O$ = $C_6H_{18}N_3O_6S_3Rh\cdot 0.75H_2O$: C, 16.35; H, 4.46; N, 9.53%.